FABRICATION OF AN ARTIFICIAL DNA NANOMOTOR OF EXTREME RUN LENGTH

ZHOU YIFAN

A THESIS SUBMITTED IN PARTIAL FULFILMENT OF THE REQUIREMENTS FOR THE DEGREE OF BACHELOR OF SCIENCE WITH HONOURS

DEPARTMENT OF PHYSICS

NATIONAL UNIVERSITY OF SINGAPORE

APRIL 2015

Acknowledgements

First and foremost, I would like to express my heartfelt gratitude to my supervisor, Professor Wang Zhisong. This thesis would not be possible without his constant guidance and encouragement. Besides patient assistance with this project, he also taught me a lot on general methodologies of scientific research as well as life lessons, which will be valuable for my life time.

I would also like to thank his lab members: Dr. Cheng Juan, Dr. Loh Iong Ying and Liu Meihan. They not only taught me the techniques of motor design and experiments, but also provided valuable thoughts during frequent discussions.

I would like to extend my gratitude to Prof. Johan Van Der Maarel, Prof. Utkur Mirsaidov and Prof. Yan Jie, who have provided useful feedback during the oral presentations.

I am also grateful to Prof. Yan Jie's lab members, who allowed me to use their 'nano drop' device and assisted with the handling.

I would also like to thank my fellow students, Chiang Yi Herng, Yeo Qing Yuan, Huang Wanjing and Onittah Lola Nair, for the insightful discussions and companionship.

Last but not least, I would like to thank the Biophysics lab Manager, Mr. Teo Hoon Hwee, and all that who had helped me with this project one way or another.

Contents

Abstract

Motor proteins are a class of biomolecules which are capable of converting chemical energy to mechanical work. Their functions are not only essential in biological processes, but also have huge potential in nanotechnology applications. However, the study of bio-systems still faces many technical difficulties, and the understanding of bio-motors is very limited. Therefore, fabrication of artificial nano-motors is attracting attention for two purposes: to produce a simplified system for further physical analysis and; to produce more effective motors for specific applications.

Prof. Wang Zhisong and his lab members have been successful in fabricating several nano-motors using DNA origami technique. These motors mimic kinasins and other bio-motors, which adopt a hand-over-hand mechanism. Nevertheless, the current products are still incomparable to bio-motors in many aspects, among which is the limited run length.

This project aims to produce a new motor with super run length. This was achieved by adopting a new mechanism: the inchworm motor. The design comprised a bridge with two G-quadruplex engines, and two legs which bind to a DNA duplex track to form triple helices. The motor was fully light driven by tethering of azo-benzenes. Azo-benzenes were tethered to the G-quadruplex engines to control the driving force. One of the legs was treated similarly to adjust the relative stability between the two legs. The combination

of the force generating engines and the asymmetry in two legs enabled the directional motion.

Fluorescence measurements were carried out to test the effectiveness of the design, as well as to investigate new possibilities brought by the inchworm motor.

List of Tables

List of Figures

Chapter 1 Introduction

1.1 Biological nanomotors

Motor proteins are a class of biomolecules that are capable of moving along the surface of a suitable substrate. They are powered by the hydrolysis of ATP (adenosine triphosphate) and convert chemical energy into mechanical work [1]. Motor proteins play a role in many biological functions: they are the driving force behind most active transport of proteins and vesicles in the cytoplasm. This is essential in many processes such as intracellular organelle transport, cell division, and muscle contraction.

Motor proteins from different category may differ in their properties. For example, actin motors such as myosin move along microfilaments through interaction with actin. Microtubule motors such as dynein and kinesin move along microtubules through interaction with tubulin. For the scope of this project, only kinesin-1 will be discussed to illustrate the operation of a bipedal molecular walker.

The operation of kinesin-1 is illustrated in Fig.1. Both legs are binding to the track in Step 1. Then, the hydrolysis of ATP and the release of phosphate provide energy to dissociate the lagging leg. In Step 3, the zippering effect will produce a forward bias to the free leg, which now becomes the leading leg. The release of ADP from a free leg and the binding of ATP to a binding leg

are spontaneous processes. After the ADP is released, the free leg will bind to the next binding site of the track spontaneously. This restores the shape in Step 1, except that the motor has moved one step forward.

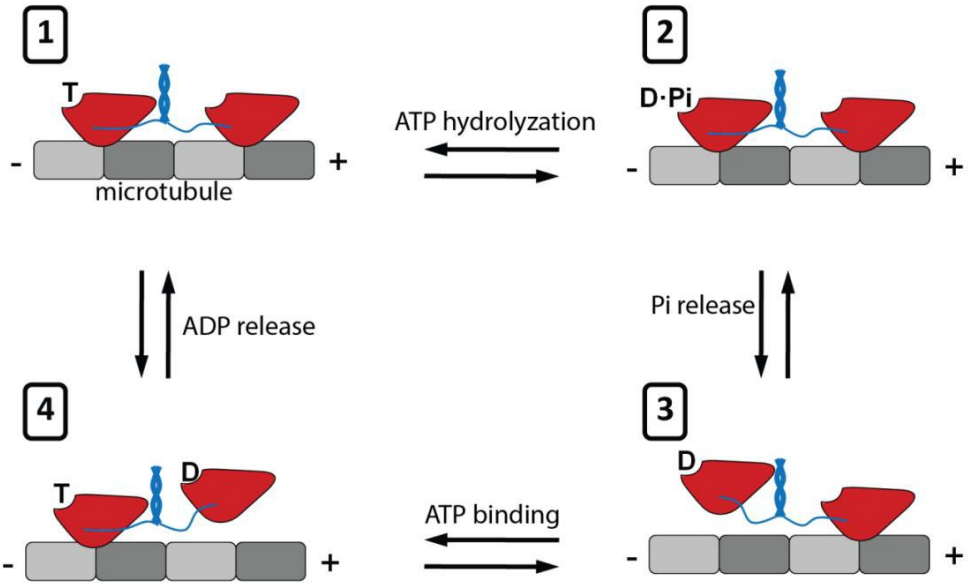

Figure 1 Mechanism of kinesin-1. [2] The two heads of the motor (red) are connected by two soft peptide chains called neck-linkers (blue). Kinein-1 moves along the microtubule (grey) in a hand-over-hand fashion.

1.2 Artificial DNA nanomotors

Due to very specific Watson-Crick base-pairing between complementary nucleotides, DNA has been recognised as a useful material in constructing nano-structures. This property has been intensely investigated in DNA origami [3]. By designing the base sequences of DNA strands, the mixture of strands (or a single strand) can be made to bind or fold into the desired shape.

Prof. Wang's lab has been successful in fabricating DNA nanomotors using the same technique. Cheng's designs mimicked the bipedal molecular walker [4][5][6]. The mechanism of these designs was very similar to that of kinesin-1 discussed above. The two legs were single stranded DNAs (ssDNA), with a section of complementary base sequence which bind together to form the neck-linker (or bridge). The track was a DNA double helix with some overhang single stranded sections, whose sequences were complementary to the legs. These overhang acted as binding sites. Instead of ATP, the fuel was a short ssDNA which could bind to the lagging leg more strongly than the binding site, hence dissociating it. The leg was then thrown forward by zippering effect, during which the fuel was cut by an enzyme, so that the leg could bind to the next binding site.

Since the early designs, more possibilities had been investigated by the lab. One of the improvements was the use of azo-benzene. By inserting azo-benzenes into a DNA strand, DNA double helices could be opened by shining UV light, and then be restored by shining visible light (detailed discussion in Chapter 2). This allowed photocontrol of the motor, which was much easier than controlling fuel concentration in the sample.

Another improvement was the modular design [7]. The idea was to untangle the energy consumption and force generating component from the motor leg. This lowered the technical requirements in motor design and directly enabled this project.

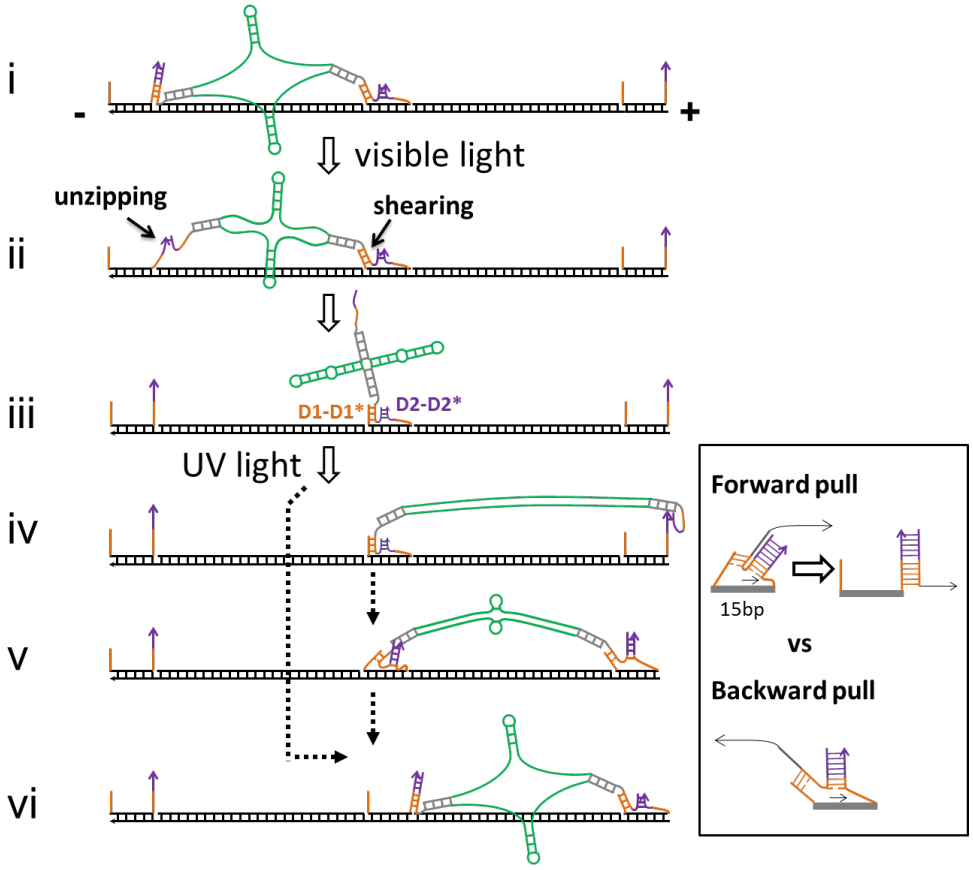

Figure 2 Mechanism of a modular nanomotor. Possible states of the DNA motor under alternating visible and UV irradiation. The inset schematically illustrates the motor's rear and front legs under opposite pulling by the winding hairpins. The rear leg is dissociated along the forward edge of the binding site and the front leg along the backward edge (the steeper edge), hence preferential rear leg dissociation [7].

Fig.2 illustrates Loh's design. By inserting azo-benzenes in the bridge, hairpins could form under visible light. The contracting bridge would exert a force on the legs, which would preferably dissociate the rear leg due to asymmetry in track design (unzipping vs. shearing forces). Under UV, the bridge would be relaxed and the free leg could bind to the next binding site. It would prefer to move to the right instead of backwards again due to asymmetric design.

This and earlier designs all adopted the hand-over-hand mechanism. The operation of hand-over-hand mechanism involves intermediate steps where only one is binding to the track. There is the risk that the second leg also dissociates and the motor fails. It is not a small risk since the legs were designed to be easily dissociable, otherwise the efficiency of the motor would have to be sacrificed.

This contradiction could be solved by the inchworm mechanism.

1.3 Inchworm motor

Inchworm mechanism was first proposed as a possible mechanism for kinesin. Later, however, mounting experimental evidence points towards the hand-over-hand mechanism as being more likely [8][9]. Since then, inchworm motor has received less attention than hand-over-hand motor. This is also partly due to technical difficulties. Nevertheless, inchworm motor still remains as a candidate in both science and application.

In contrast to the hand-over-hand motor, where the two legs lead each other alternately, the inchworm motor has one leg always leading the other. This characteristic allows us to confine the legs round the track in order to overcome the problem discussed and to achieve super run length. In fact, such confinement, which prevents position exchange of the two legs, is a prerequisite of any implementation of inchworm motor.

Dan Li et al. discussed a general implementation of inchworm motor and carried out computer simulations [10]. This design was inspired by studies on molecular shuttles, where a shuttle ring could be switched back and forth between a pair of binding sites (Fig. 3A). They proposed a motor consisting of two such rings and a bridge with controllable length. The motor could move forward in inchworm manner by coordination of the three controls: tighten the lagging leg, loosen the leading leg, and extend the bridge; now the leading leg would be pushed one step forward; then tighten the leading leg, loosen the lagging leg, and shorten the bridge; now the lagging leg would be pulled one step forward, and that completed one cycle.

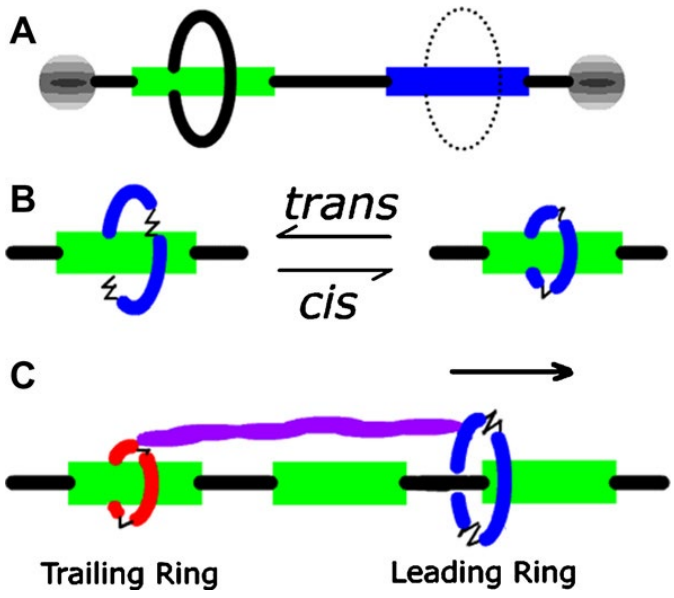

Figure 3 Schematic of a ring-shaped inchworm motor [10]. (A) Illustration of a shuttle system. (B) A proposed mechanism for operating on a ring to regulate its affinity to an extended track with identical binding sites. (C) A twin-ring walker.

Efficiency of the motor could be analysed using Langevin dynamics. Since the motion was only allowed along the track, the end-to-end distance of the bridge polymer (R), approximately satisfies the one-dimensional Flory potential:

$$\mathrm{F(R)} = k_B T \left(b\frac{N^2}{R} + \frac{R^2}{N B^2}\right)$$

where b is the effective Kuhn length of the bridge polymer and N is the number of Kuhn monomers. The bridge ' s intra-chain diffusion was simulated using the Verlet algorithm. Motion of a mobile ring is described by Langevin equation:

$$m\frac{d^2r}{dt^2} = f(t) - m\gamma\frac{dr}{dt} + f_R$$

where $\mathrm{f} = \frac{\partial \mathrm{f}}{\partial \mathrm{r}}$ is the force due to the intra-chain potential, and $\mathrm{f_R}$ is the stochastic force and γ is friction coefficient.

Although Li et al. did not fabricate the motor, they carried out computer simulation using reasonable parameters and the results displayed directional motion.

1.4 Framework of thesis

1.4.1 Scope and objectives of thesis

The aim of this thesis is to design and fabricate an inchworm motor, and to experimentally test its effectiveness as well as investigating its properties. Although inchworm mechanism was adopted in order to achieve super run length, it was only tested with three-binding-site track due to technical difficulties and time constraint.

The focus is to judge the success or failure of the motor from the translocation signal of fluorescence measurements.

1.4.2 Outline of thesis

Chapter 1 covers some background on artificial nanomotor. It introduces the importance of this field, the past achievements upon which this thesis is based, as well as the motivation of this thesis.

Chapter 2 provides an overview of G-quadruplex, DNA triple helices and azobenzene which are essential components in motor design.

Chapter 3 demonstrates the proposed design of the inchworm motor. The difficulties and possibilities of this design are also discussed.

Chapter 4 demonstrates the experimental methodologies, including techniques of annealing, gel electrophoresis and fluorescence measurements. Experimental results are summarised and discussed in Chapter 5.

Chapter 6 summarises and reviews the work throughout the thesis. Some future works are also suggested to explore the potential of this design.

Chapter 2 Overview

2.1 Introduction

This chapter gives an overview on essential structures used in the motor design. The track in this design was a fully complementary double stranded DNA (dsDNA), while the two legs of the motor were ssDNA of appropriate sequences which could bind to the binding sites on the track through DNA triple helices. Two G-quadruplex engines were included in the bridge, which generate force and drive the motor. Azobenzenes were inserted in G-quadruplex engines and one of the legs (azo-leg), which enabled photocontrol of the motor.

2.2 DNA triple helices

DNA triple helices have displayed much potential in various applications, and have unsurprisingly attracted lots of attention [11]-[17]. A DNA triplex is formed when pyrimidine or purine bases occupy the major groove of the DNA double Helix forming Hoogsteen pairs with purines of the Watson-Crick basepairs. Intermolecular triplexes are formed between triplex forming oligonucleotides (TFO) and target sequences on duplex DNA.

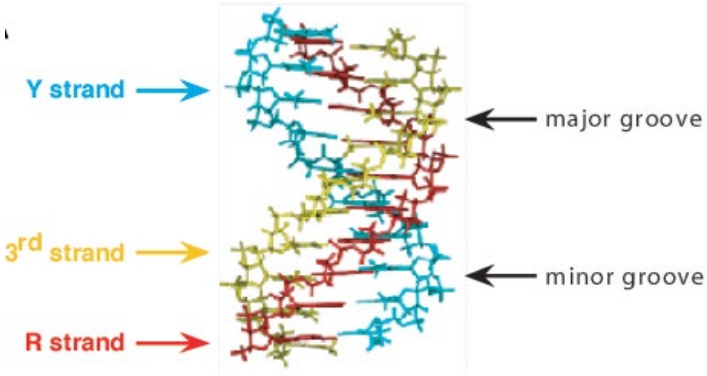

Figure 4 Structure of DNA triplex [12]. The third strand is in yellow, whereas the oligopurine and the oligopyrimidine strand are respectively in red and blue.

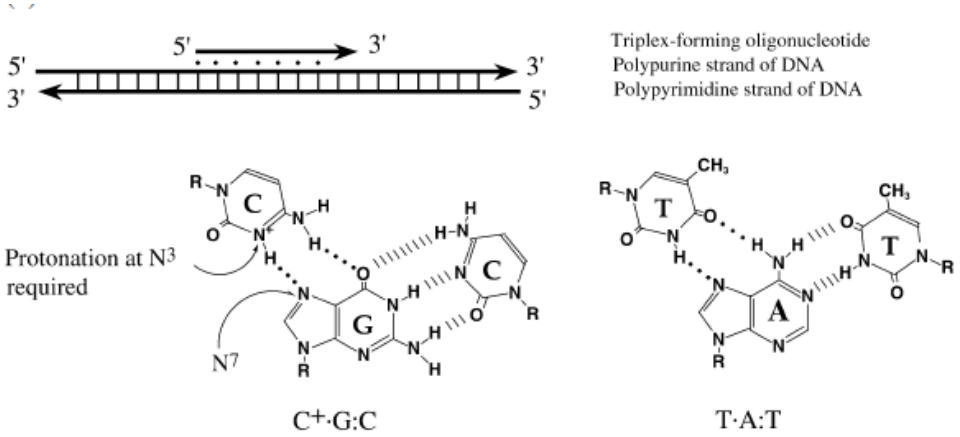

Figure 5 YRY triplex motif [15]. Triplex formation occurs at polypurine–polypyrimidine sites in duplex DNA. In the YRY motif, the third strand is parallel in polarity to the purine strand of the duplex. The canonical base triplets are also shown.

Although some other combinations are also allowed (e.g. reverse Hoogsteen), the YRY motif (pyrimidine. purine: pyrimidine) is found to be

most stable, where a homopyrimidine TFO binds to a homopurine.homopyrimidine section of duplex.

Stability of DNA triplex is often modeled in a three-state experiment [18]-[20], where the triplex dissociates to duplex plus TFO and then to three ssDNA with increasing temperature:

$$Triplex \overset{K_3}{\Leftrightarrow} Duplex + TFO \overset{K_2}{\Leftrightarrow} Coils$$

State: 3 2 1

The fraction of triplex Θ_3 is then given by:

$$\Theta_3 = \frac{K_2 K_3 c(1 - \Theta_3)}{K_2 K_3 c(1 - \Theta_3) + K_2 + 1}$$

By parameter fitting with the experimental data an equation about stability can be obtained:

$$K_{eq} = \exp\left[\left(\frac{1}{R}\right)\left(\frac{\Delta H - \Delta G_{37}}{310} - \frac{\Delta H}{T}\right)\right]$$

where T is temperature, ΔH is enthalpy change, ΔG_{37} is standard free energy at 37℃. The latter two are functions of base sequence with empirical parameters.

Besides base sequence, triplex stability is also sensitive to pH [21][22] and cation concentration [23][24]. This allows plenty of room in fine tuning of the motor.

The kinetics [25]-[28] and rupture force [16][29] of DNA triplex are within the timescale of the experiment and strength of G-quadruplex engine respectively. The details, however, are not very relevant since those experiments were carried out under very different condition. The feasibility of a specific sequence can only be tested through experiments.

2.3 G-quadruplex engine

G-quadruplexes are nucleic acid sequences that are rich in guanine and are capable of forming a four-stranded structure. They are relatively stable, polymorphic, yet with well-defined conformations [30][31]. These properties have made them a potential structure in nanodevices.

Amongst other applications, a specific design is of special interest to this project, where it shifts between quadruplex and duplex conformation reversibly to produce extension and contraction (Fig. 6).

The G-quadruplex (G-4) section is a 21-base oligonucleotide, with four groups of three guanines and will form quadruplex structure spontaneously. C-fuel is complementary to G-4 but with a few mismatch. Since duplex structure is thermodynamically more stable, C-fuel can bind to G-4 and open it despite the mismatch. G-fuel is fully complementary to C-fuel; it can bind to C-fuel

through the overhang, and open the binding between C-fuel and G-4. The single stranded G-4 will then form quadruplex again.

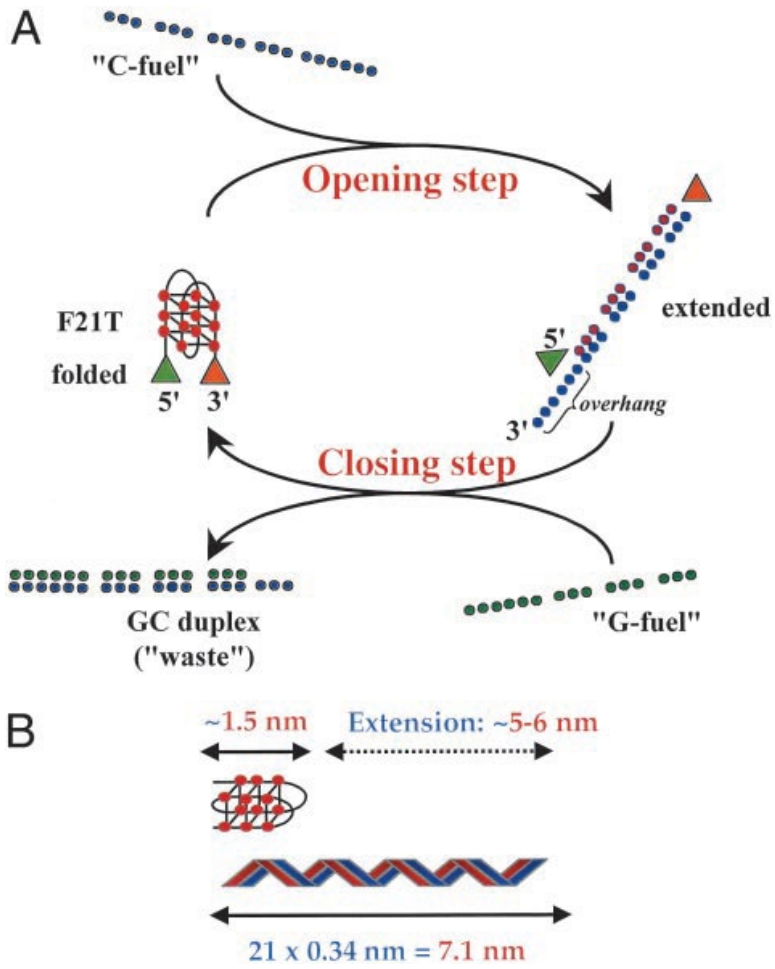

Figure 6 G-quadruplex engine [32]. (A) Switching between an intramolecular quadruplex (left) and a duplex (right). (B) Induced movement.

2.4 Azobenzene

An azobenzene unit contains a C=C double bond, whose isomerization can be controlled by light: it shifts to trans-stereoisomer under visible light, and to cis-stereoisomer under UV light. What makes it interest is that, when tethered to DNA strands, it takes the position and orientation such that it stabilizes DNA duplex in trans-state through intercalating effect, while destabilizes DNA duplex in cis-state due to steric hindrance [33][34]. As a result, stability of DNA duplex can be adjusted by light.

In the motor design, azobenzenes were tethered to C-fuel of G-4 engine. In this way, C-fuel can be dissociated without the need of G-fuel, and becomes reusable by switching between UV and visible light.

Furthermore, research has shown that azobenzenes have the same effect on DNA triple helix [35]. By tethering azobenzenes to the motor leg, leg control proposed in Section 1.3 can be achieved.

Chapter 3 Motor design

3.1 Schematic

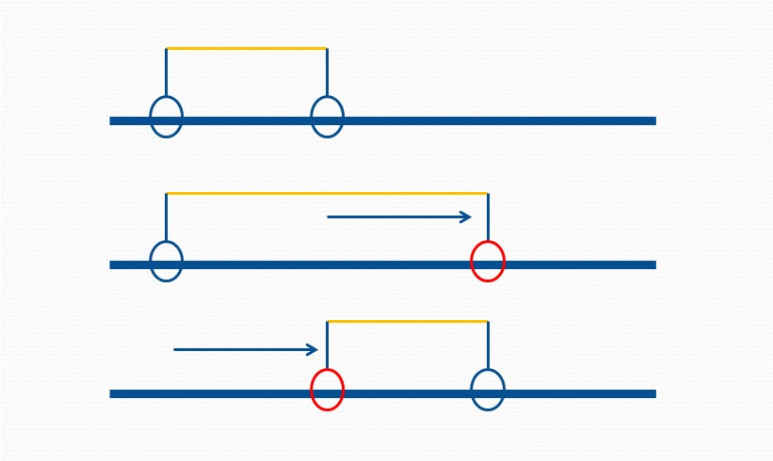

Figure 7 Schematic of motor design. The motor comprises a controllable bridge (yellow) and two legs (thin blue). The track is thick blue. The rings mean that legs are confined around the track. The red ring means that the leg is dissociated but still confined.

The schematic illustrates the operation of inchworm motor, which also sets forward the requirements. In the first step, the bridge extends, while the leading leg is less stable, hence pushing it forward. In the second step, the bridge contracts, while the lagging leg is less stable, hence pulling it forward. The initial shape is restored, and the motor has moved forward along the track.

Three requirements must be met in order to have a feasible design:

1. The bridge needs to be controllable. This was achieved by incorporating G-quadruplex engines in the bridge.

2. The legs need to be confined around the track all the time. This was achieved by adding two additional ssDNA to form closed loops around the track.
3. The relative stability of two legs needs to be adjusted. This was achieved by tethering azobenzenes to one of the leg (azo-leg). A series of TFO sequences had been tested by Liang et al. [35], amongst which the one that produced the largest difference between stabilities under UV and visible light was chosen: XT_6XT_7, where X denotes an azobenzene and T_6 denotes a block of six Thymine. This TFO has a melting temperature of 48.4 ℃ under visible light, while that is below 0 ℃ under UV. Another sequence was chosen for non-azo-leg (or normal leg), CTCCTTT, with a melting temperature of 18.6℃ [21]. As a result, the azo-leg is more stable than the normal leg under visible light, while less stable under UV.

Attention should be paid here that these melting temperatures are not very accurate for this design, since they were measured by different groups under different buffer conditions and structures. The normal leg sequence was purposely chosen to have slightly lower melting temperature than experiment temperature (25℃), since the number was expected to be higher in this design due to entropy penalty of confinement. Nevertheless, the differences between the three melting temperatures were quite significant and allowed a safe buffer zone.

3.2 Detailed design

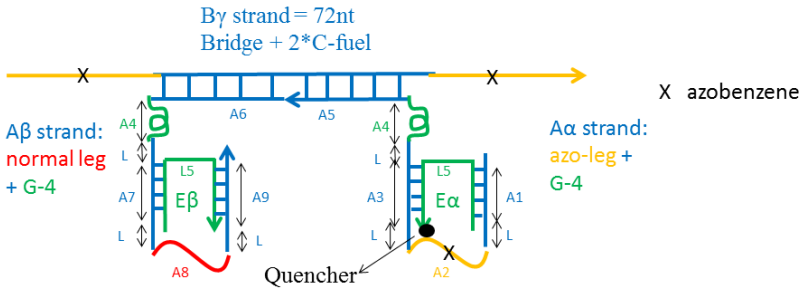

Figure 8 Detailed motor design. A α , A β and B γ strands form the motor.

B γ strand comprises a 30nt (nucleotides) bridge (A5+A6), with a C-fuel sequence added to each end (yellow straight). A α and A β bind with B γ strand through double helix (A5, A6 sections respectively). A α includes the azo-leg (A2) and a G-4 engine (A4). A β includes normal leg (A8) and the other G-4 (A4). E α is a closing strand that binds to A α through two sections (A1 and A3) each of 10bp length. E β has similar structure but binds to A β through (A7 and A9). L is 2nt linker and L5 is 5nt linker. Azo-leg and C-fuel sections are tethered with azobenzenes (denoted by X; actual number of azobenzenes at each section varies; refer to Section 4.1) . E α strand carries a quencher at 3' end..

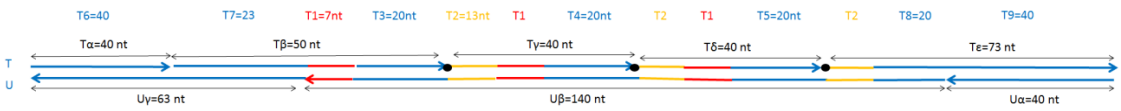

Figure 9 Track design.
T1 (red) are binding sites for normal leg, T2 (yellow) are binding sites for azo-leg. They are separated the 20nt spacers of different sequences. A long

section is added to each end of the track so that motor can be trapped instead of leaving the track. The three black dots are fluorescent dyes. They are Texas Red (TEX), CY5, and TYE from left to right.

3.3 Motor operation mechanism

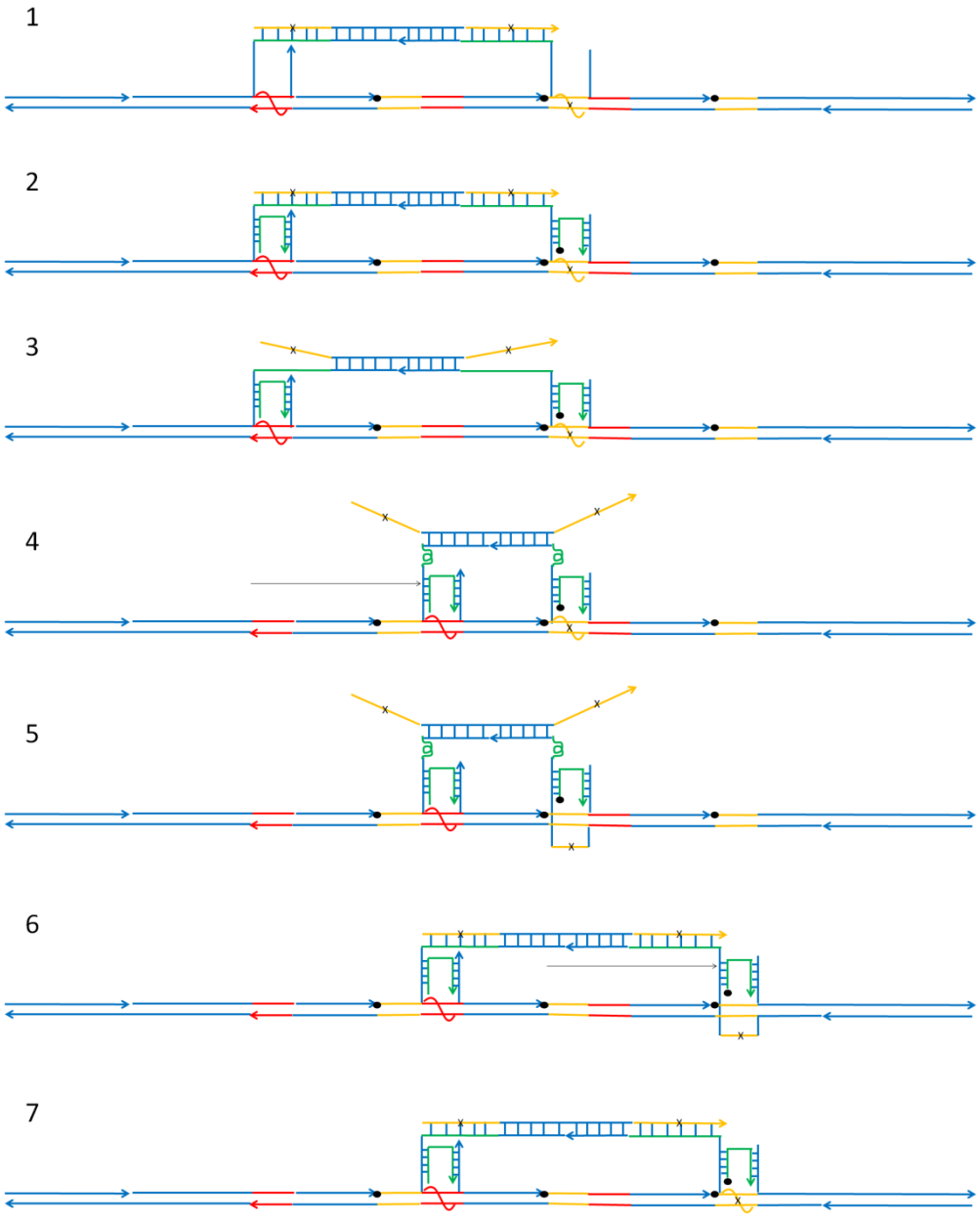

Figure 10 Motor mechanism.

In Step 1, motor binds to the track. The case illustrated has all three azobenzenes in trans-state. The real situation was more likely a mixture. In Step 2, closing strands are added which bind to the motor and form closed loop around the track. These two steps illustrate the binding process before the operation. In Step 3 -5, UV is switched on; C-fuels are dissociated and G-4 engines contract; triplex has slower reaction rates and azo-leg only dissociates later. In Step 6 and 7, light is switched to visible; C-fuels bind to and open G-4 engines; again, azo-leg reacts more slowly.

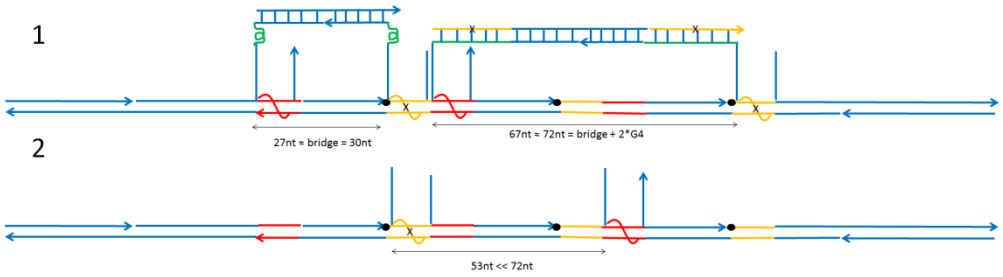

Figure 11 Initial binding direction.

The length of the bridge of motor and spacers of track were designed to facilitate one binding direction over the other. Fig. 11.1 illustrates comfortable binding position for both short state and long state, while the reverse binding would incur large tension. Even if the azobenzenes are initially in random state, reverse binding is unfavourable compared with forward binding since only one binding position is possible (Fig.11.2).

3.4 Direction control

The direction of the motor movement is determined by relative reaction rates between the G-quadruplex engine and azo-leg. In Section 3.3, it is assumed that G-quadruplex responds faster than the azo-leg. It can be easily seen that if the opposite is true, the direction will be reversed. In fact, that was the original assumption when this motor was designed. The kinetic data from the references are not directly comparable since they were measured under different structure and buffer condition. As a result, it was hard to predict the direction of motor at the beginning of this project. After the direction of motor was confirmed from experiments, current interpretation was arrived that G-quadruplex responds faster than the azo-leg in this design and buffer condition.

But this special characteristic brings more than confusion. The subtle competition between reaction rates opens the possibility of easy direction control by small changes in environment.

Chapter 4 Experimental Methodology

4.1 Sequence design

Sequences of essential components were already decided, which were G-4 engine, C-fuel, motor legs and binding sites. The rest of the sequences also required some careful works to avoid undesired binding and self-folding, which would hinder annealing.

These sections were firstly filled with sequences from lambda DNA [36], which is a phage whose natural structure is largely single stranded. The full sequences were then tested with mfold [37] and unpack [38]. These two are online tools which can compute and predict the secondary structures of a given sequence. Based on the results, sequences were then modified base by base to minimise any undesired structure.

Strand	Length	Sequence
Aα	75	GGGTGGCGAGaaXTTTTTTXTTTTTTTaaGAGTTGGTATttG GGTTAGGGTTAGGGTTAGGG TTTATTATTTATGAA
Aβ	69	AATTTTGAGGTTTGT GGGTTAGGGTTAGGGTTAGGGttATTATGTTAGttCTCCTTT aaGTCGTGTATG
Eα	25	CTCGCCACCCtttttATACCAACTC-/3IAbRQSp/

Eβ	25	CTAACATAATttttCATACACGAC
Bγ	72	CCXCTXAAXCAXCTXAAXCGXCTXAAXGCC ACAAACCTCAAAATTTTCATAAATAATAAA CCXCTXAAXCAXCTXAAXCGXCTXAAXGCC
Tα	40	TCATAACTTAATGTTTTTATTTAAAATACCCTATGAAAAG
Tβ	50	AAAGGAAACGACAGGTGCTGAGG GAGGAAA GGAATGAACAATGGAAGTAA-3' - /TEX615/
Tγ	40	TTTTTTTTTTTTTGAGGAAA CCTTTCGGTGGCTGGCTTAC-3'-/Cy5/
Tδ	40	TTTTTTTTTTTTTGAGGAAA CGAGTATTGGCACCATTAAG-3' - /TYE563/
Tε	73	TTTTTTTTTTTTT AGGTTGGATAGGGAGGTTGA TGGTATTCTTAGAGGCGGTGGCAAGGGTAATGAGGTAGA T
Uα	40	ATCTACCTCATTACCCTTGCCACCGCCTCTAAGAATACCA
Uβ	140	TCAACCTCCCTATCCAACCTaaaaaaaaaaaaaCTTAATGGTGC CAATACTCGTTTCCTCaaaaaaaaaaaaaGTAAGCCAGCCACCG AAAGGTTTCCTCaaaaaaaaaaaaaTTACTTCCATTGTTCATTCC TTTCCTC
Uγ	63	CCTCAGCACCTGTCGTTTCCTTTCTTTTCATAGGGTATTTT AAATAAAAACATTAAGTTATGA

Table 1 DNA sequences. X denotes azobenzenes.

4.2 Motor fabrication

Sequences with azobenzene tethering were ordered from Nihon Techno Service Co., Ltd. The rest were ordered from Integrated DNA Technologies, Inc. The DNA samples received were in lyophilized form. They were then resuspended in TE buffer (10 mM Tris, 0.1 mM EDTA, pH 8.0) and refrigerated under -20℃.

A calculated amount of each strand was taken out from the stock solution, mixed together, and diluted to 5uM for annealing. Annealing buffer used was 20mM $MgCl_2$, 100mM KCl, in TE. The samples were annealed in water bath at 95℃ for 20 minutes, after which they were cooled down slowly until room temperature, followed by storage under 4℃.

4.3 Gel Electrophoresis

After the samples were annealed, polyacrylamide gel electrophoresis (PAGE) was carried out to verify the effectiveness of annealing.

29:1 30% acrylamide (ml)	H_2O (ml)	10× TBE (ml)	10% APS (μl)	TEMED (μl)
4	6.6	1.2	200	10

Table 2 Composition of 10% acrylamide gel.

The gel was cast using Mini-PROTEAN Tetra cell setup. A pair of glass plates was thoroughly cleaned with DI water and 70% ethanol. They were then carefully installed onto the holder. The 10% acrylamide gel was prepared in fume hood according to Table 2. TEMED was the last to add, after which the gel was quickly pipetted into that glass plates. A comb was inserted carefully to avoid any bubbles. The gel was then left in the fume hood for 50 minutes for it to solidify.

Around 4-6 ul of samples were prepared with Gel Loading Dye, Orange (6X), as well as a sample of low molecular weight DNA ladder, both by New England BioLabs. The gel was then installed in the tank and filled with 1x TBE. The samples were pipetted into the wells, and the power supply was set to 90V and 70 min.

After that, the gel was stained with 3x gel red for 20 minutes and then imaged with the Bio-Rad Gel Doc EZ system.

4.4 Fluorescence measurements

Three fluorescent dyes were attached to the track, which would produce fluorescence signal under excitation of appropriate wavelength. On the other hand, the closing strand at azo-leg carried a quencher, which can quench the nearby fluorescent dye through fluorescence resonance energy transfer

(FRET). As a result, the ratio between the fluorescence readings from a track/motor mixture sample and a pure track sample is related to the percentage occupation of the binding site by the motor. By monitoring the relative change in three binding sites, the movement of the motor along the track could be observed. An added benefit of this experiment was that it minimised (hopefully removed) the effect of photobleaching, which was expected to have similar effects on both samples.

Such experiments had become more convenient with the utilisation of azobenzenes. The light source inside the fluorospectrometer could provide sufficient intensity and appropriate wavelength to induce isomerisation of azobenzenes. By setting alternating visible and UV sessions, the fluorespectrometer would drive the motor while taking fluorescence measurements during visible sessions.

Before operation experiment, the motor must bind to the track (Fig.10.1-2). Motor and track samples at 5uM were mixed 1:1 and incubated overnight. On the second day, equal amounts of 5uM closing strands were added to the mixture, and also incubated overnight.

Before each experiment, the cuvette was rinsed with 70% ethanol for two times, followed by twenty times of DI water. The sample was diluted to 10nM using operation buffer (in this case the same as annealing buffer).

The excitation wavelengths of the three dyes were 648nm (Cy5), 549nm (TYE) and 596nm (TEX), which were suitable to induce cis-trans isomerisation of azobenzenes based on previous experience from lab members. The excitation slit was set to 360nm for UV sessions, which was efficient in inducing trans-cis isomerisation. The slit width was set to 5nm (Ex.) and 10nm (Em.).

Chapter 5 Results and discussion

5.1 Gel electrophoresis

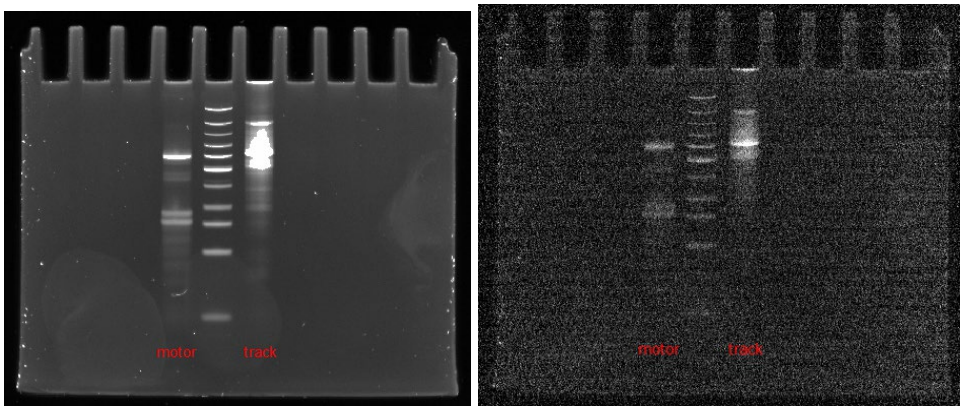

Figure 12 Electrophoresis. The same gel under longer (left) and shorter (right) exposure. From left to right lanes are: motor sample, ladder, track sample.

A clear band could be seen from both motor and track. Pictures were taken at two exposure due to large difference in intensity. In this experiment, the track was diluted to half the concentration of motor sample, a smaller volume was taken as well. In spite of this, its intensity was still much stronger than the motor, mainly due to the large difference in molecular weight.

The motor was at around the same distance as the track. This was probably a coincidence. The secondary structure of motor was quite messy, including a large component of ssDNA and some quadruplexes, while the track was a dsDNA. As a result, the relative position of the motor could not reflect its relative molecular weight.

To verify this, a stepwise annealing and gel electrophoresis was carried out, where two of the three motor components were annealed together. The lower bands from the motor sample were evidently contributed by other structures resulting from incomplete annealing, and the highest and brightest band was referred to be the designed motor structure.

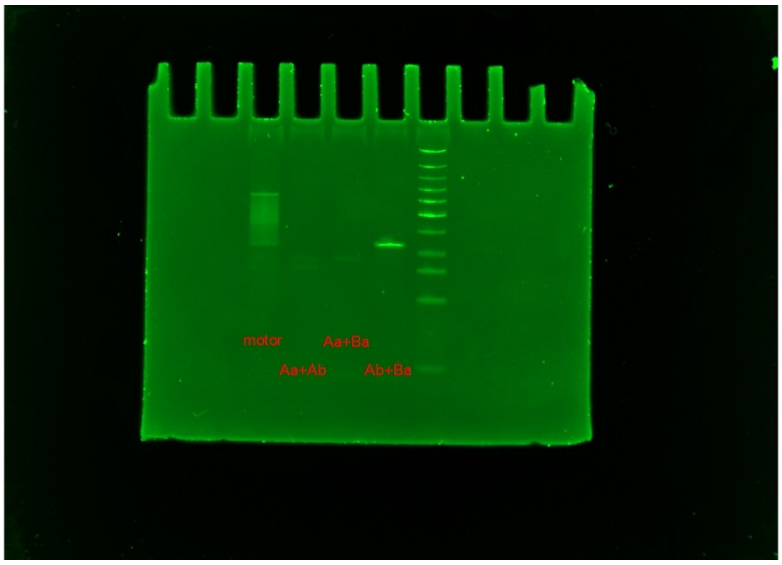

Figure 13 Stepwise electrophoresis. From left to right: full motor (A α +A β +B α), A α +A β , A α +B α , A β +B α .

5.2 Motor binding

The binding of this motor took two steps: the motor/track binding and the binding of closing strands (Fig.10.1-2).To ensure equilibrium was achieved, each step was incubated overnight. The fluorescence spectrum was measured after binding, and compared with that of a pure track sample. A compare experiment was also carried out, where the sequence of mixture was changed: in the first step, motor was mixed with closing strands to form structure in Fig.8; track was added later after overnight incubation.

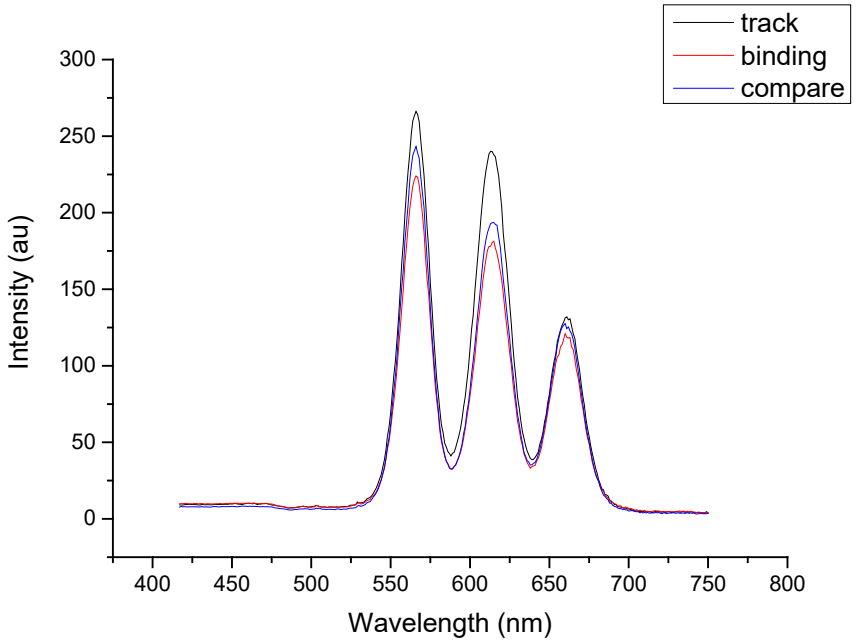

Figure 14 Motor binding. The fluorescence spectrum of pure track (black), binding sample (red) and the compare sample (blue). Three peaks from left to left are TYE, TEX, CY5.

From the data, intensities at all three peaks were lowered after binding, demonstrating that motor bound to the three binding sites and the fluorescent dyes were quenched. The intensities from the compare experiment lied in between, demonstrating that binding were still possible after the loops were formed, but less favourable. The difference between the binding experiment and the compare showed that the desired binding structure was formed under normal binding procedure, where motors bound to track first followed by loop closing around the track.

5.3 Motor operation

For operation experiments, fluorescence was measured over time at three wavelengths, which were the peaks from the spectrum. Fig.14 illustrates a sample data, as well as how it was analysed to produce meaningful information. For each experiment, three lines were obtained from the three fluorescent dyes. There were no reading during UV sessions, and they were removed from timeline to have a clean presentation. By dividing control readings with the operation readings, the ratio should reflect the percentage of binding sites unoccupied by motor. By subtracting the initial value, the data showed the change in percentage occupation during the experiment, which reflected the movement of motor.

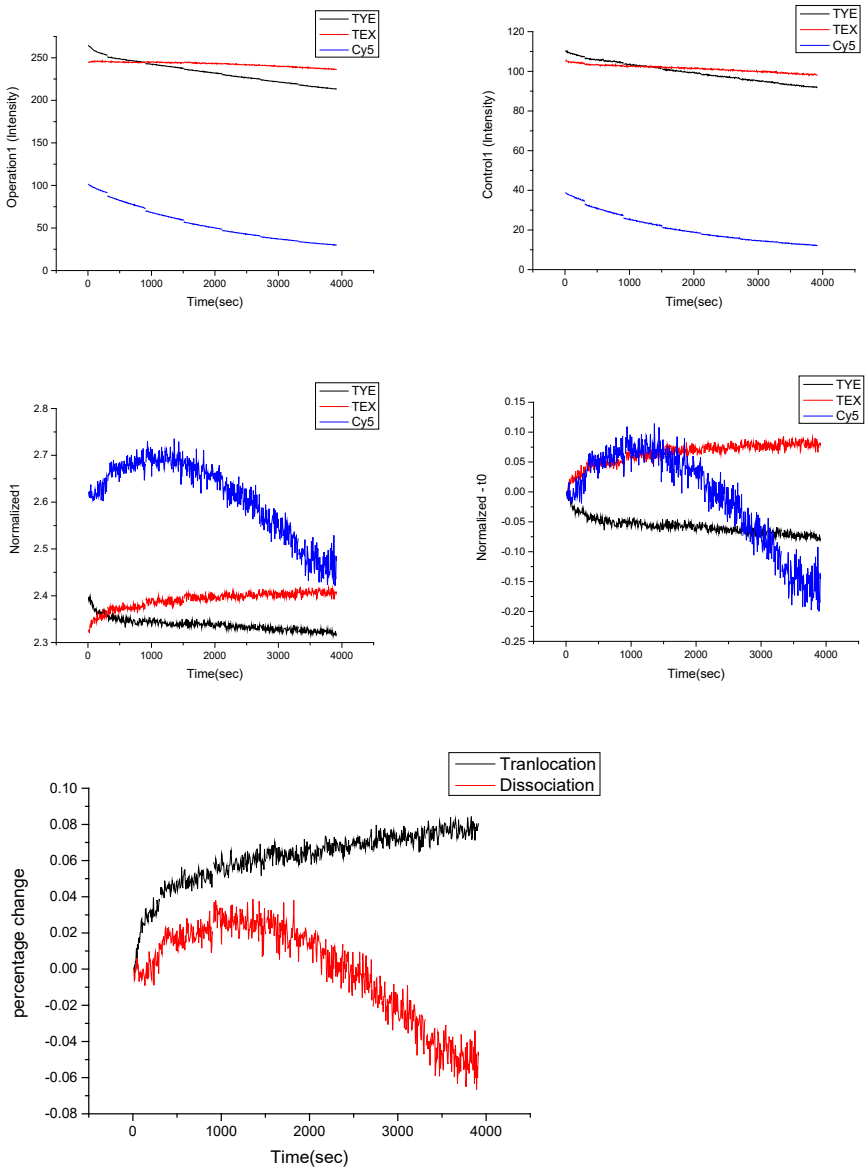

Figure 15 Motor operation. From top to bottom, left to right: fluorescence intensity of operation sample, fluorescence intensity of control (pure track), the ratio between operation and control readings, the ratio minus the initial value, translocation and dissociation.

In Fig.14.4, all three lines started at 0, which was the reference level. After the light source was turned on and as time propagates, intensity from fluorescent dye TEX (red) increases, while intensity from TYE (black)

decreases. This demonstrated that the motor – and the quencher with it – left the minus end, where TEX became less quenched, and arrived at plus end, where TYE became more quenched. The Cy5 (middle dye) signal will be discussed in Section 5.3.

Quality of the motor could be more clearly presented by two quantities (Fig.14.5). Translocation was calculated as half the difference between TEX (minus end) and TYE (plus end), which measured the efficiency of this motor. Overall dissociation was calculated as the average of three dyes, which was inversely related to run length.

The data shown in Fig.14 was obtained with a 10/10 procedure, which means that each operation cycle comprised 10 minutes of visible light and 10 minutes of UV, and repeated for six cycles. Experiments were also carried out with other procedures; a comparison can be made to investigate the properties of this motor under different procedures.

Procedure		No. of experiments	Translocation	Overall dissociation
Visible	UV			
5 min	10 min	2	0.035986	0.003194
10 min	10 min	3	0.117825	-0.06182
20 min	20 min	2	-0.00141	0.107712
30 min	30 min	4	0.037216	-0.03897

Table 3 Comparison across procedures. Translocation and overall dissociation were taken as the average of the last ten values of each experiment. Repeated experiments were carried out for each procedure; the data displayed was the average.

The motor displayed highest translocation and lowest dissociation under 10min/10min procedure. Interestingly, it worked second best under 30min/30min, and the worst under 20min/20min. This seemed to suggest that the influence of procedure was quite complicated and the efficiency of the motor had a turning point between 10/10 and 30/30. It was also possible to be caused by experimental errors, since 20/20 was less repeated.

5.4 Uncertainties

One major trouble was that fluorescence intensity of pure track dropped quickly after taking out of refrigerator and kept in the lab under 25℃. These samples were taken out for two days before control experiment because the binding took two days for this motor. From several tests, the intensity dropped to around half after one day, and to around a quarter after two days. A new sample was annealed with newly prepared buffer, and the problem remained. The dropping was slowed down or stopped after binding; as a result, the operation readings were higher than control readings (Fig. 14).

Since little was known about this effect, it was uncertain if this control experiment could correctly take care of the effect. Data was also analysed using another control, where the track sample was only taken out of refrigerator one hour before the experiment. For the 10min/10min procedure, overall dissociation became higher with this control, yet the directionality

remained clear. It is therefore fairly safe to conclude that that motor was successful under this procedure.

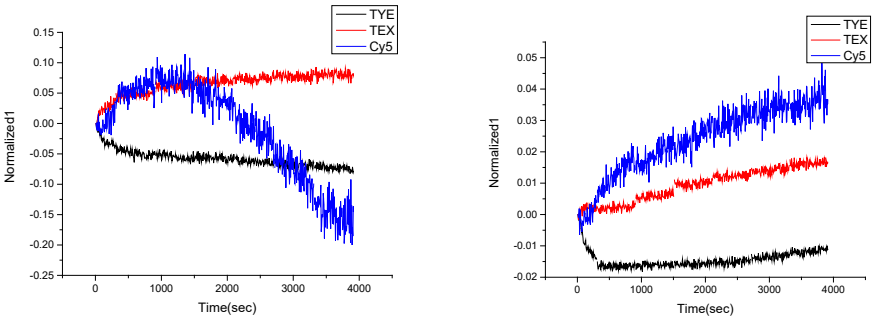

Figure 16 Control comparison. Data processing using two-day control (left) and one-hour control (right)

When one-hour control was applied to 30min/30min procedure, however, the results suggested a reversed direction. If this control was justified, it would imply that the direction of this motor could be reversed simply by changing the procedure. Although this control has not been proven yet, such delicate direction control is not impossible. As discussed in Section 3.4, this motor is quite sensitive to environment and stimuli. Besides, longer session time might increase the influence of thermodynamic properties over kinetic properties in determining the direction of motor, leading to more complex analysis.

Another problem was the behaviour of middle dye (Cy5). This was not a new problem, as the middle dye signals had been hard to interpret in most of previous projects in this lab. It might reflect some strange thermodynamic properties of the design or a limitation in experimental technique.

Chapter 6 Conclusion and outlook

6.1 Conclusion

An inchworm motor was designed in order to achieve super run length. Its legs bound to the track through DNA triple helix, with G-quadruplex engines generating force. Photocontrol was achieved through tethering of azobenzenes. The motor was then fabricated and tested experimentally.

Although there were unexpected problems, the motor was fairly successful as it displayed clearly directional movement. The motor had been tested under different procedure, and it was most efficient under 10min visible/ 10min UV cycles. It also displayed low dissociation under10min/10min and 30min/30min cycles, which was in line with super run length.

6.2 Outlook

As a motor designed to have super run length, it may exhibit more surprising performance on longer track. Many exciting possibilities were revealed during design and experiments, and further works are required to fully explore its potential. Fine tuning of design, buffer condition and procedures will not only improve its efficiency, but may open the possibility of easy direction control.

On the other hand, the intensity dropping of the track and other uncertainties may also require some effort so that more accurate experiment could be carried out to investigate this delicate device.

Bibliography

1. Schliwa M. (ed). Molecular Motors. (2003) Wiley-VCH Verlag GmbH & Co. KGaA, Weinheim, FRG.
2. R. Hou, PhD Thesis, NUS, 2013.
3. Zadegan, R.M.; Norton, M.L (2012). "Structural DNA Nanotechnology: From Design to Applications". Int. J. Mol. Sci 13: 7149–7162.
4. J. Cheng, S. Sreelatha, R. Hou, A. Efremov, R. Liu, J. R. C. van der Maarel, and Z. Wang, "Bipedal Nanowalker by Pure Physical Mechanisms," Phys. Rev. Lett., vol. 109, no. 23, p. 238104, Dec. 2012.
5. J. Cheng, S. Sreelatha, I.Y. Loh, R. Hou, Z. Wang, "Autonomous artificial nanomotor integrating ratchet and power stroke for efficient utilization of single fuel molecules," Phys. Rev. Lett, under external review.
6. R. Hou, J. Cheng, S. Sreelatha, J. Wei, Z. Wang, "Autonomous synergic control of a nanomotor, " ACS Nano, under external review.
7. IY. Loh, PhD Thesis, NUS, 2014.
8. Yildiz A, Tomishige M, Vale RD, Selvin PR (2004). "Kinesin Walks Hand-Over-Hand".Science 303 (5658): 676–8.
9. Asbury CL (2005). "Kinesin: world's tiniest biped". Current Opinion in Cell Biology 17 (1): 89–97.
10. D. Li et al., Chemical Physics 352 (2008) 235 – 240.
11. Y.-K. CHENG and B. M. PETTIT, STABILITIES OF DOUBLE- AND TRIPLE-STRAND HELICAL NUCLEIC ACIDS, Prog. Biophys. raolec. Biol., Vol. 58, pp. 225-257, 1992
12. Maria Duca et al., The triple helix: 50 years later, the outcome, Nucleic Acids Research, 2008, Vol. 36, No. 16 5123 – 5138
13. Maxim D. Frank-Kamenetskii, Sergei M. Mirkin, TRIPLEX DNA STRUCTURE, Annu.R ev. Biochem1. 995. 64:65-9.
14. Cherny et al., Analysis of Various Sequence-Specific Triplexes by Electron and Atomic Force Microscopies, Biophysical Journal Volume 74 February 1998 1015–1023
15. K. M. Vasquez and P. M. Glazer, Triplex-forming oligonucleotides: principles and applications, Quarterly Reviews of Biophysics 35, 1 (2002), pp. 89–107.
16. Ling et al., Rupture Force between the Third Strand and the Double Strand within a Triplex DNA, J. AM. CHEM. SOC. 2004, 126, 13992-13997
17. Jungkweon Choi and Tetsuro Majima, Conformational changes of non-B DNA, Chem. Soc. Rev., 2011, 40, 5893–5909
18. G. Eric Plum and Kenneth J. Breslauer, Thermodynamics of an Intramolecular DNA Triple Helix: A Calorimetric and Spectroscopic Study of the pH and Salt Dependence of Thermally Induced Structural Transitions, J. Mol. Biol. (1995) 248, 679–695

19. E. Protozanova and R. B. Macgregor, Jr., Kinetic Footprinting of DNA Triplex Formation, ANALYTICAL BIOCHEMISTRY 243, 92–99 (1996)
20. RICHARD W. ROBERTS AND DONALD M. CROTHERS, Prediction of the stability of DNA triplexes, Proc. Natl. Acad. Sci. USA Vol. 93, pp. 4320–4325, April 1996
21. Leitner et al., Influence of Sequence-Dependent Cytosine Protonation and Methylation on DNA Triplex Stability, Biochemistry 2000, 39, 5886-5892
22. G. Manzini et al., Triple Helix Formation by Oligopurine-oligopyrimidine DNA Fragments Electrophoretic and Thermodynamic Behavior, J. Mol. Biol. (1990) 213,833-843
23. S.W. Blume et al., The integral divalent cation within the intermolecular purine*purine·pyrimidine structure: a variable determinant of the potential for and characteristics of the triple helical association, Nucleic Acids Research, 1999, Vol. 27, No. 2 695–702
24. Thresia Thomas and T. J. Thomas, Selectivity of Polyamines in Triplex DNA Stabilization, Biochemistry 1993, 32, 14068-14074
25. P.J. Bates et al., Detection and kinetic studies of triplex formation by oligodeoxynucleotides using real-time biomolecular interaction analysis (BIA), Nucleie Acids Research, 1995, Vol. 23, No. 18 3627-3632
26. Luigi Emilio XODO, Kinetic analysis of triple-helix formation by pyrimidine oligodeoxynucleotides and duplex DNA, Eur. J. Biochem. 228, 918-926 (1995)
27. L.J. Maher et al., Kinetic Analysis of Oligodeoxyribonucleotide-Directed Triple-Helix Formation on DNA, Biochemistry 1990, 29, 8820-8826
28. Rougee et al., Kinetics and Thermodynamics of Triple-Helix Formation: Effects of Ionic Strength and Mismatches, Biochemistry 1992,31, 9269-9278
29. Chang et al., Direct visualization of triplex DNA molecular dynamics by fluorescence resonance energy transfer and atomic force microscopy measurements, Applied Physics Letters 91, 203901 (2007)
30. Aboul-ela, F., Murchie, A. I. H. & Lilley, D. M. J. (1992) Nature 360, 280–282.
31. Williamson, J. R. (1994) Annu. Rev. Biophys. Biomol. Struct. 23, 703–730.
32. Alberti and Mergny, DNA duplex–quadruplex exchange as the basis for a nanomolecular machine, PNAS, February 18, 2003, vol. 100, no. 4, 1569–1573
33. Liang et al., Supra-photoswitch Involving Sandwiched DNA Base Pairs and Azobenzenes, small 2009, 5, No. 15, 1761–1768
34. Asanuma et al., Nucleic Acids Symposium Series No. 49, 35-36
35. Liang et al., Photoregulation of DNA Triplex Formation by Azobenzene, J. AM. CHEM. SOC. 9 VOL. 124, NO. 9, 2002 1877
36. Sanger et al. 1982 J. Mol. Biol. 162: 729-773
37. M. Zuker, Mfold web server for nucleic acid folding and hybridization prediction. Nucleic Acids Res. 31, 3406–3415 (2003).
38. J. N. Zadeh et al., J. Comput. Chem., in press, doi:10.1002/jcc.21596.